




ARTICLE

Open Access

# TPU-assisted adhesive PDMS film for dry or underwater environments

Sangyeun Park <sup>1</sup>, Minhyeok Kim <sup>1</sup> and Hongyun So <sup>1,2</sup>

## Abstract

Adhesive polymer films with anisotropic properties on either side have attracted tremendous interest for biomedical and engineering applications. However, developing an innovative solution that provides effective adhesion under both dry and wet conditions remains a considerable challenge. In this study, we devised a novel process for creating adhesive films by casting polydimethylsiloxane (PDMS) onto a thermoplastic polyurethane (TPU) substrate. During the curing process, the PDMS layer in contact with the TPU was lightly cross-linked, which significantly increased adhesion. The catalytic reaction used for polymerization was regulated by the TPU, which is known to adsorb metal ions. This adhesive PDMS film (APF) demonstrated outstanding adhesion on various substrates under dry and underwater conditions and maintained adhesion even after repeated use. In practical applications, the APF proved to be an effective waterproof patch by adhering to the surfaces of objects submerged in water.

## Introduction

Numerous unique adhesion phenomena occur in nature, such as in gecko foot hairs<sup>1</sup>, mussels<sup>2</sup>, and the suction cups of octopi<sup>3,4</sup>, which have inspired the design of many adhesives with strong and reusable adhesion. Among these, reusable adhesives that can be used in both dry and underwater environments have attracted significant attention owing to their high demand in daily life and industrial applications<sup>5</sup> as epidermal adhesives<sup>6</sup>, underwater sensors<sup>7</sup>, and water leak repairs<sup>8</sup>. To enhance their usability, the adhesives must possess sufficient mechanical properties and exhibit strong adhesion to various substrates. Among the diverse adhesives, tape adhesives<sup>9,10</sup>, which provide direct adhesion of substrates, offer better reusability than glue adhesives<sup>11</sup>. However, tape adhesives with multilayer structures that combine rigid carriers and soft adhesives often exhibit poor mechanical properties and poor interfacial adhesion

between different materials<sup>12,13</sup>. Therefore, it is imperative to develop robust tape adhesives that can be reused multiple times.

Polydimethylsiloxane (PDMS) is commonly used as a stretchable substrate and waterproof packaging material because of its transparency<sup>14</sup>, hydrophobicity<sup>15</sup>, and flexibility<sup>16,17</sup>. Owing to these useful characteristics, efforts have been made to utilize PDMS as an adhesive by enhancing adhesion through manipulation of the cross-linking networks<sup>18,19</sup>. The cross-linking network affects the stiffness and surface adhesion of a material<sup>20</sup>. Notably, the networks in PDMS can be controlled by modifying the amount of curing agent, adjusting the thermal curing conditions, or adding chemicals<sup>21,22</sup>. Additionally, hydrosilylation of PDMS can be interrupted by inhibitors<sup>23</sup> when the prepolymer is mixed with oligomers<sup>16</sup>, surfactants<sup>24</sup>, or amine-based materials<sup>25</sup>. However, fully cross-linked PDMS exhibits good stiffness but poor surface adhesion, whereas PDMS with lightly cross-linked chains exhibits good adhesion but reduced mechanical strength<sup>9</sup>. Therefore, an adhesive PDMS that exhibits both excellent mechanical properties and high adhesion remains a key requirement for applications in numerous fields.

Correspondence: Hongyun So ([hyso@hanyang.ac.kr](mailto:hyso@hanyang.ac.kr))

<sup>1</sup>Department of Mechanical Engineering, Hanyang University, Seoul 04763, South Korea

<sup>2</sup>Institute of Nano Science And Technology, Hanyang University, Seoul 04763, South Korea

These authors contributed equally: Sangyeun Park, Minhyeok Kim

© The Author(s) 2024



**Open Access** This article is licensed under a Creative Commons Attribution 4.0 International License, which permits use, sharing, adaptation, distribution and reproduction in any medium or format, as long as you give appropriate credit to the original author(s) and the source, provide a link to the Creative Commons licence, and indicate if changes were made. The images or other third party material in this article are included in the article's Creative Commons licence, unless indicated otherwise in a credit line to the material. If material is not included in the article's Creative Commons licence and your intended use is not permitted by statutory regulation or exceeds the permitted use, you will need to obtain permission directly from the copyright holder. To view a copy of this licence, visit <http://creativecommons.org/licenses/by/4.0/>.

Herein, we report adhesive PDMS films (APF) with different adhesion strengths obtained by simply tuning the PDMS chains on the surface during curing. The side of the PDMS in contact with thermoplastic polyurethane (TPU) during the curing process was lightly cross-linked and exhibited a higher adhesion strength. In contrast, the other side of the cured PDMS film normally had highly cross-linked chains and a higher modulus. The APF, a soft wet-adhesive film, uniformly adhered to various substrates with rough and flat structures while being deformed along their surfaces. Owing to these characteristics, the proposed adhesive is suitable for use in waterproof patches, wearable sensors, and grippers for underwater applications. Furthermore, the APF, which has a simple production method, is amenable to large-scale manufacturing and can be applied in various industrial environments.

## Experimental procedure

### Materials

The PDMS-based elastomer Sylgard 184 (Dow Corning, United States), which consists of a silicone base and a curing agent, was used. The TPU film was purchased from Jinheung Industry (South Korea) and was made from polymeric glycol and polyisocyanate. In addition, a platinum (Pt) catalyst solution (with a platinum(0)-1,3-diene-1,1,3,3-tetramethyldisiloxane complex) was purchased from Sigma-Aldrich.

### Preparation of adhesive PDMS

In our approach, the only modification relative to conventional PDMS processing was the use of TPU as a substrate for curing the PDMS. The TPU substrate was cleaned with isopropyl alcohol (IPA) for degreasing and dust removal. Subsequently, the substrate was washed with deionized (DI) water and dried using an air dryer. The PDMS precursor was prepared by mixing the base PDMS and curing agent at a ratio of 10:1. The precursor was then degassed under vacuum for half an hour and poured onto the substrate. The curing conditions were 6 h at 40 °C, 4 h at 60 °C, and 2 h at 80 °C. The films produced at curing temperatures of 40 °C, 60 °C, and 80 °C were denoted as 40APF, 60APF, and 80APF, respectively. A thick acrylic plate cut into the desired design was used to control the thicknesses and shapes of the samples. The designed acrylic plate was stacked on top of the TPU film and secured with screws to serve as a mold.

### Preparation of normal PDMS

A normal PDMS film (NPF) was prepared using the same process used for the APF. The only difference in the process was the substrate used for curing the PDMS precursor. For the NPF, an acrylic material was utilized as the substrate in the curing process instead of a TPU film.

Furthermore, the films produced at curing temperatures of 40 °C, 60 °C, and 80 °C were denoted as 40NPF, 60NPF, and 80NPF, respectively.

### Mechanical properties

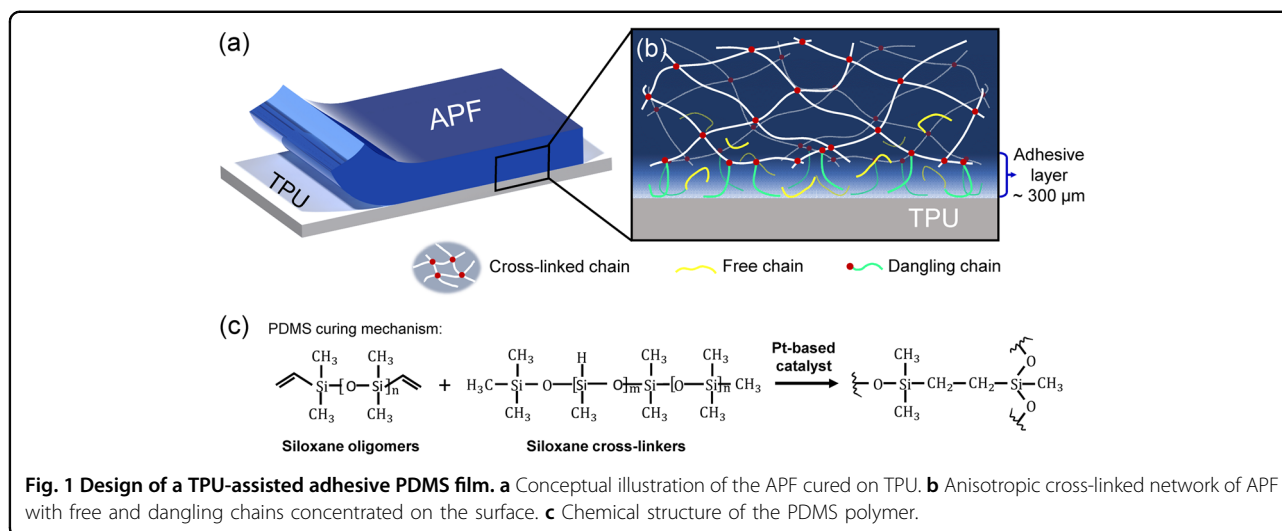
Tensile tests were conducted using a tensile and compressive testing machine (MCT-2150, A&D Co.). The samples had thicknesses of 4.5 mm and widths of 10 mm, and the gauge lengths of the bulk PDMS were 40 mm. The tensile speed was maintained at 100 mm/min, and Young's modulus was obtained from the linear-range slope of the stress-strain curves at 20% strain. At least three tests were conducted for each sample type.

### Adhesion tests

Normal adhesion tests were conducted through a tack test using a tensile and compressive testing machine<sup>26</sup>. The samples had areas of 2 cm × 2 cm and thicknesses of 5 mm. A custom-made probe head was prepared for each sample. The samples were firmly attached to the probe head of the testing machine, which had the same area as the sample. Due to the nonadhesive nature of the opposite side of the sample, the side of the sample to be attached to the head was treated with an oxygen plasma and then semipermanently fixed to the head with superglue. The conditions for the normal adhesion tests included testing speeds of 20 mm/min to 40 mm/min and preloads of 5 N to 20 N. The adhesive properties of the PDMS films under dry conditions were evaluated with various substrates, including aluminum (Al), glass, Si wafers, polylactic acid (PLA), polyethylene terephthalate (PET), and TPU. The adhesion properties with varying surface roughnesses were tested with an acrylonitrile butadiene styrene (ABS) substrate manufactured using a fused filament fabrication three-dimensional (3D) printer. The underwater adhesion properties of the adhesive PDMS films were evaluated on different substrates, including Al, Si wafers, and PLA. All substrates used in the tests were cleaned with IPA, washed with DI water, and dried. Cyclic tests were conducted under both dry and underwater conditions with a load of 5 N for 20 cycles at a test speed of 20 mm/min. In the preloading test, the load range was varied from 1 N to 50 N, and the test speed was maintained at 20 mm/min. Creep tests were conducted under both dry and underwater conditions by attaching a 200 g weight to the APF with a 20 N load for 5 s and then measuring the hanging time. A minimum of three tests were conducted with each adhesion test condition to ensure reliable results.

### Material characterization

Raman spectra in the range 50–3400 cm<sup>-1</sup> were obtained with a laser wavelength of 532 nm and a micro-Raman spectrometer (DXR-3xi, Thermo Fisher Scientific) installed at the Hanyang LINC3.0 Analytical Equipment



Center (Seoul). The measurement parameters included a laser power of 10 mW, an exposure time of 0.02 s, and 1000 scans. For Raman mapping, the same spectrometer was used with specific settings: a laser power of 10 mW, exposure time of 0.083 s, image pixel size of 2  $\mu\text{m}$ , 5 scans, and an image size of 100  $\mu\text{m}$   $\times$  500  $\mu\text{m}$ .

To quantitatively determine the concentrations of Pt atoms, inductively coupled plasma–mass spectrometry (ICP-MS, Agilent 7700 Series ICP-MS, Agilent Technologies) was used with a quadrupole and dual-mode discrete dynode electron multiplier. The sample used in the analysis was diluted 200 times by adding deionized water (DI water) as a background solution, and the concentration was calculated as follows:

$$\text{Concentration} = \frac{(\text{measured value} - \text{background value})}{\times \text{dilution factor}} \quad (1)$$

### Contact angles

Contact angle (CA) measurements were performed on a CA goniometer (Phoenix-MT(A) Surface Electro Optics, Korea) with image analysis software (Image-Pro 300). Water droplets with volumes of 7.32  $\mu\text{l}$  were employed for the measurements. The CAs were evaluated on PET, Si wafers, glass, Al, 3D-printed PLA, and TPU substrates. Additionally, the CA of the PDMS surface was also measured. Screenshots were captured immediately after the water droplet was placed, and at least three positions on each surface were tested. The obtained data were averaged and reported with standard derivations.

### Morphological analyses

To evaluate the surface roughness of the substrate, an alpha-step profilometer (Dektak-XT, Bruker) was used. Furthermore, scanning electron microscopy (SEM;

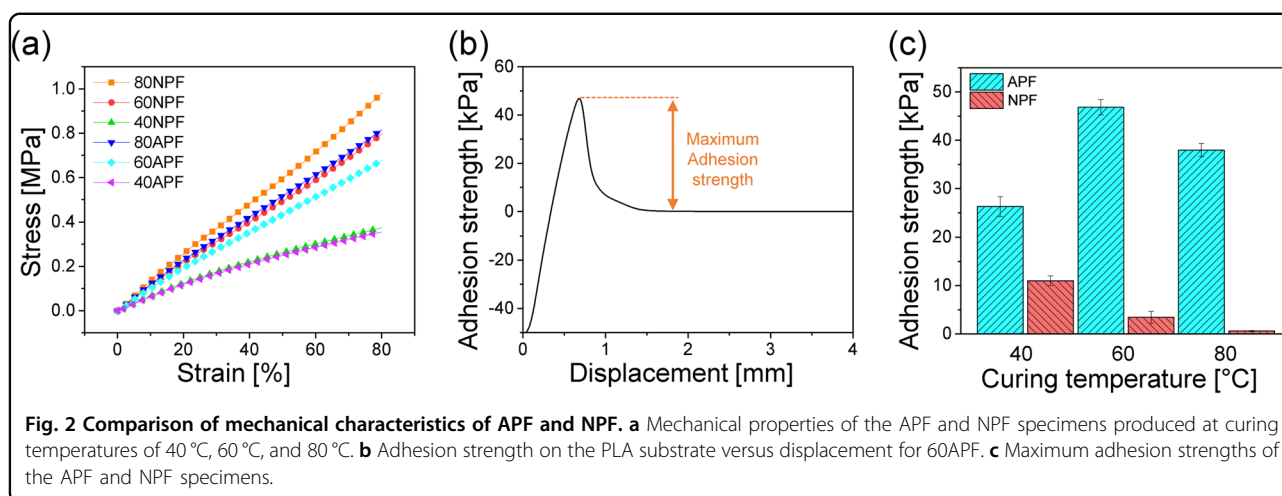
Quattro ESEM, Thermo Scientific) was used to identify the bonded areas in the bulk PDMS.

## Results and discussion

### Design and characterization of the adhesive films

Figure 1a shows a schematic of an APF fabricated on a TPU separated from a substrate. The APF was simply fabricated by curing a conventional PDMS precursor on a TPU substrate. The PDMS precursor was prepared by mixing the base and curing agent. The base PDMS contained double-ended vinyl PDMS and a Pt catalyst<sup>27,28</sup>, while the curing agent consisted of many Si-H bonds and may also contain other oligomers<sup>29,30</sup>. During the curing process, the vinyl PDMS in the base and the Si-H bonds in the curing agent formed a highly cross-linked network through hydrosilylation catalyzed by the Pt catalyst (Fig. 1c). The cured PDMS is contained three types of polymer networks: free chains, dangling chains, and cross-linked chains<sup>31</sup>. The free chains were unbound and mobile in the polymer network, the dangling chains were connected at only one end with a deformable other end, and the cross-linked chains were connected at both ends and strongly fixed in the network. Notably, the anisotropic distribution of the polymer chains led to varying mechanical and adhesive properties of the APF (Fig. 1b). The loosely cross-linked network, which was rich in free and dangling chains, exhibited excellent stickiness and softness despite its low elastic modulus. To characterize the mechanical properties affecting adhesion, tensile tests of both NPF and APF were conducted using a tensile testing machine (Fig. S1a).

Figure 2a shows the stress–strain curves for specimens 40NPF, 40APF, 60NPF, 60APF, 80NPF, and 80APF. As the curing temperature increased, the Young's modulus of bulk PDMS increased linearly<sup>22</sup>. In comparing the moduli of NPF and APF, Young's moduli of 60APF and 80APF



were approximately 16% lower than that of NPF (Table S1). This may be due to the soft adhesive gel on one side of the APF surface. The normal adhesion test, illustrated in Fig. S1b, was conducted as a tack test. The testing process for the PDMS film samples is detailed in Fig. 2b and Fig. S2. Positive values indicated a tensile adhesion strength, whereas negative values indicated a compressive preloading strength. The maximum adhesion strength was defined as the maximum force divided by the contact area, which was measured when the film detached from the surface after applying a preload. The maximum adhesion strengths of the films are shown in Fig. 2c. For each sample with different curing temperatures, as the curing temperature decreased, the modulus also decreased, making it easier to deform under the same applied force. When the sample deformed to match the surface topology of the substrate, the contact area increased, potentially increasing the adhesion strength. Consequently, the adhesive strengths of the NPFs increased in the order 80NPF, 60NPF, and 40NPF based on the change in modulus. In considering the adhesive properties of APF, we considered the influence of the bulk PDMS modulus and the unique properties of the soft adhesive gel. The surface adhesion of APF was higher overall than that of NPF due to the adhesive gel formed on the surface of APF. The 60APF exhibited an excellent adhesion strength of 47 kPa, which was approximately 13.6 times greater than that of 60NPF. Similarly, 80APF demonstrated a greater adhesion strength (38 kPa) than 80NPF. However, 40APF exhibited a relatively low adhesion strength due to its low intrinsic modulus and weak properties, so it was unable to provide strong adhesion on the surface.

#### Raman spectra of the PDMS films and raw materials

To examine the source of APF adhesion, we used Raman spectroscopy to analyze the network changes in PDMS induced by TPU. Figure S3a shows a comparison

of the Raman spectra of the NPF and APF specimens cured at 60 °C. Overall, the peaks and intensities of the films were approximately similar. However, compared with that of APF, the Raman band at  $1600\text{ cm}^{-1}$  for NPF was weaker, indicating the presence of C = C bonds in the vinyl groups<sup>32,33</sup>. This variation arose from consumption of the vinyl groups during the cross-linking reaction, which led to a decrease in the peak intensity<sup>32</sup>. Hence, the results suggested that the surface of the APF was not fully cross-linked, indicating that it contained many lightly cross-linked networks, such as dangling and free chains (Fig. 1b). To characterize the depth of the lightly cross-linked layer, spatial variations in the vinyl groups (C = C bonds) in the cross-section of the APF were determined with Raman spectral mapping. As shown in Fig. S3b, the intensity of the peak increased as the position approached the surface. The peak intensity up to a depth of approximately  $300\text{ }\mu\text{m}$  was greater than that of the NPF, indicating that the adhesive layer existed at that depth. In addition, reduced cross-linking of the APF may be due to a shortage of the Pt catalyst. To confirm this, the effect of the adhesive gel on the APF surface was investigated. The Raman spectra of the condensed gel were compared with those of the base PDMS and curing agent (Fig. S3c). The bands of the gel and base PDMS yielded very similar spectra; a slight difference was observed in the  $2160\text{ cm}^{-1}$  peak, which was attributed to the formation of Si-H bonds<sup>34</sup>. This implied that the gel was simply a mixture of the base PDMS and the curing agent rather than due to the introduction of any other substances.

Interestingly, when the PDMS was cured in direct contact with the TPU, the Pt atoms in the PDMS migrated and adhered to the surface of the TPU. The donor atoms in the functional groups of TPU adsorbed the heavy metals, M(II), through coordinate bonds<sup>35</sup>. Therefore, the Raman peak at  $1539\text{ cm}^{-1}$  in the spectrum of the TPU film was attributed to N-H bonds, which



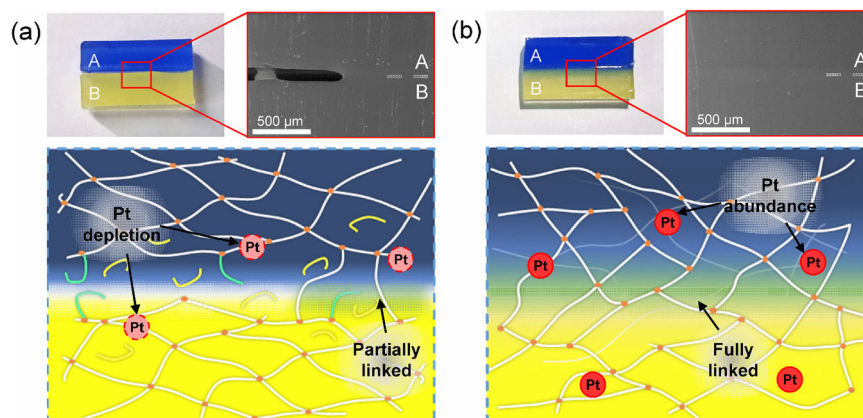


**Fig. 3** Differences in cross-linking reactions at the interface of double PDMS. Optical and SEM images of double PDMS and schematic illustration of the cross-linked network; (a) 'A' region, which is the APF (shown in blue in the optical image), and subsequently added PDMS ('B' region); (b) 'A' region, which is the NPF (shown in blue in the optical image), and the subsequently added PDMS ('B' region).

served as binding sites for the Pt atoms present in the base PDMS<sup>33,36</sup> (Fig. S4). Pt adsorption by the TPU film was also demonstrated through ICP-MS analysis. The Pt atoms in the TPU film before PDMS casting were below the detection limit. In contrast, Pt atoms were detected in the TPU film used as the substrate for PDMS casting and cleaned with DI water and IPA, as shown in Table S2. Consequently, the Pt atoms detected in the TPU film were transferred from the PDMS.

To clarify the influence of the Pt catalyst, double PDMS was fabricated, in which the precursor was successively added to APF and NPF. Figure 3 shows optical and SEM images of the double PDMS. The initially fabricated PDMS (APF or NPF) is depicted in blue, and the subsequently added PDMS is depicted in yellow (Fig. S5a). The 'A' region, which is the APF (shown in blue in the optical image), and the subsequently added PDMS ('B' region) formed a partially bonded interface due to the lack of a Pt catalyst (Fig. 3a). In contrast, the 'A' region, which was NPF, and the other 'B' region were completely bonded to each other after curing (Fig. 3b). Finally, the Pt catalyst was directly added to the condensed gel to complement the PDMS curing inhibition mechanism. As shown in Fig. S5b, the gel was completely cured after mixing, confirming that Pt depletion caused by TPU was an inhibiting factor. Subsequently, the adhesive properties of the PDMS were measured as a function of the Pt catalyst content. The samples were prepared by adding varying amounts of Pt catalyst to the PDMS precursor and then curing on acrylic substrates. Comparing the addition of 10  $\mu$ l and 20  $\mu$ l of the Pt catalyst to NPF, the adhesion strength was lower in the sample with the Pt catalyst added (Fig. S5c). This showed that the Pt catalyst content affected the adhesive properties of PDMS.

#### Dry adhesion strength of the adhesive film

The adhesive properties in dry environments were characterized under various conditions, as shown in Fig. 4. For qualitative characterization, additional investigations were conducted using samples fabricated at a curing temperature of 60  $^{\circ}$ C for 4 h. To determine the adhesive properties under dry conditions, the maximum adhesion strengths of APF and NPF for each type of substrate were measured using a normal adhesion test, as shown in Fig. 4a<sup>37,38</sup>. The test setup is illustrated in Fig. S1b. Notably, the adhesive strength of APF was greater than that of NPF for all substrates. APF exhibited the strongest adhesion (34.8 kPa) to the PET surface, followed by the Si wafer, glass, Al, PLA, and TPU. Moreover, it is noteworthy that the APF demonstrated remarkably higher adhesion strengths on substrates with rough surfaces, such as 3D-printed PLA, for which the adhesion strength was approximately 7.71 times greater than that of NPF. The lightly cross-linked side with many dangling and free chains was more deformable, allowing the APF to better adhere to rough surfaces and creating stronger adhesion by increasing the contact area<sup>9</sup>. Subsequently, the adhesion strength was measured as a function of the surface roughness of the substrate<sup>39,40</sup>. To regulate the surface roughness, four types of substrates with different patterns were fabricated using 3D printing technology with ABS filaments. As shown in Fig. S6, the differences in the shapes of the surface patterns of the four substrates were measured using an alpha step profilometer. Figure 4b shows a comparison of the maximum adhesion strength with respect to the surface roughnesses. Furthermore, the tests were performed with a small preloading force of 5 N and a large preloading force of 50 N. The adhesion strength increased as the size of the surface pattern on the substrate decreased from 400  $\mu$ m to 200  $\mu$ m, because the

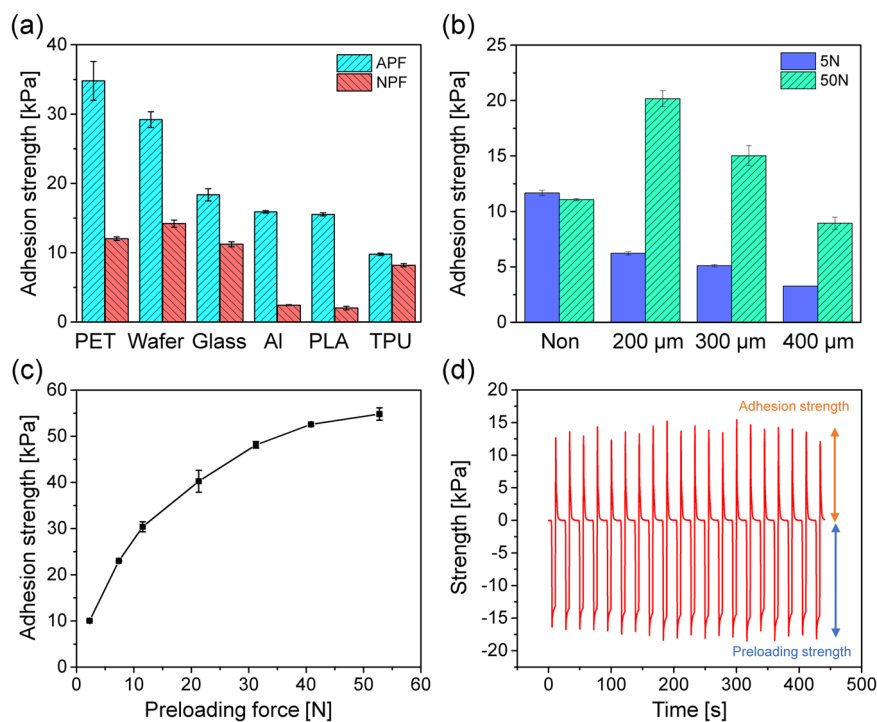


**Fig. 4 Adhesion of the PDMS film in a dry environment.** **a** Adhesion strengths of the APF and NPF specimens on various substrates including PET, wafers, glass, Al, PLA, and TPU. **b** Adhesion strengths of the APF on substrates with different surface patterns depending on the preloading force. **c** Effect of the preloading force on the adhesion strength of the APF. **d** Cyclic adhesion test of the APF specimen.

contact area of the APF attached to the substrate increased. In addition, as the preloading force increased from 5 N to 50 N, the adhesion strength of the substrate with a surface pattern increased, whereas the substrate without a surface pattern showed similar adhesion strengths in both cases. This is because in the case of substrates without surface patterns, the contact areas over which APF adhered to the substrate did not change even if the preloading force was increased. However, for substrates with surface patterns, when the preloading force was increased, the contact area at which the APF adhered to the substrate increased, as shown in Fig. S7. Additionally, Fig. S8a shows optical images of APFs adhered to various substrates, including PET, Si wafers, glass, Al, PLA, and TPU, under dry conditions. In addition, the results confirm that 1 kg and 2 kg weights were adhered and lifted with the APF (Fig. S8b). These results demonstrated excellent APF adhesion to various substrates under dry conditions.

To determine the adhesive properties of APF under various preloads, the maximum adhesion strength was obtained by gradually increasing the preloading force (1 N to 50 N) used to attach the APF to the PLA substrate. As shown in Fig. 4c, as the preloading force increased, the adhesion strength generated by peeling off the APF attached to the substrate increased. This was because

when the preloading force increased, the adhesive gel of the APF deformed along the shape of the substrate surface, resulting in better adhesion. Figure S7 illustrates that as the preloading force increased, the APF underwent more pronounced deformation along the shape of the substrate surface, resulting in an increased contact area. To examine the reusability of the APF under dry conditions, cyclic tests were performed in which the APF was attached and detached 20 times from the PLA substrate, as shown in Fig. 4d. Here, positive values indicated the adhesion strength, whereas negative values indicated the preloading strength. The results showed that similar adhesion strengths were maintained during the cyclic tests, thereby confirming that APF was reused without a loss in adhesive strength. Furthermore, when a 200 g weight was attached to the APF for creep tests, it lasted  $359 \pm 28$  s. The cycling tests and creep tests demonstrated reversible adhesion of the APF under dry conditions.

#### Underwater adhesion performance of the adhesive film (influence of surface wettability)

Prior to characterizing underwater adhesion by APF, the effects of the surface wettabilities of various substrates on wet adhesion were investigated. As shown in Fig. 5a and Fig. S9, CAs were obtained for substrates comprising different materials. Among these substrates, the Si wafer,

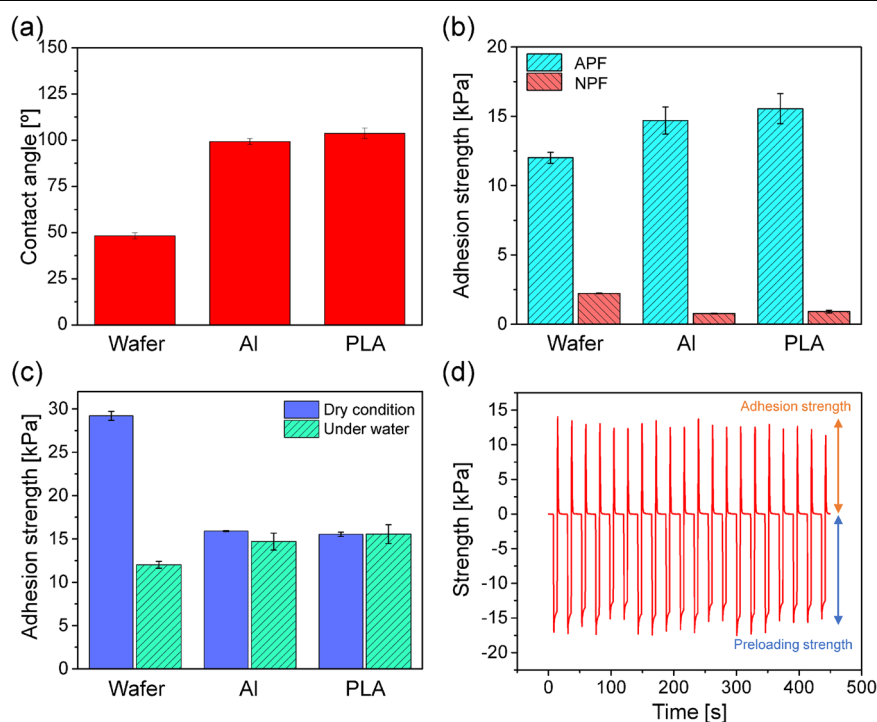
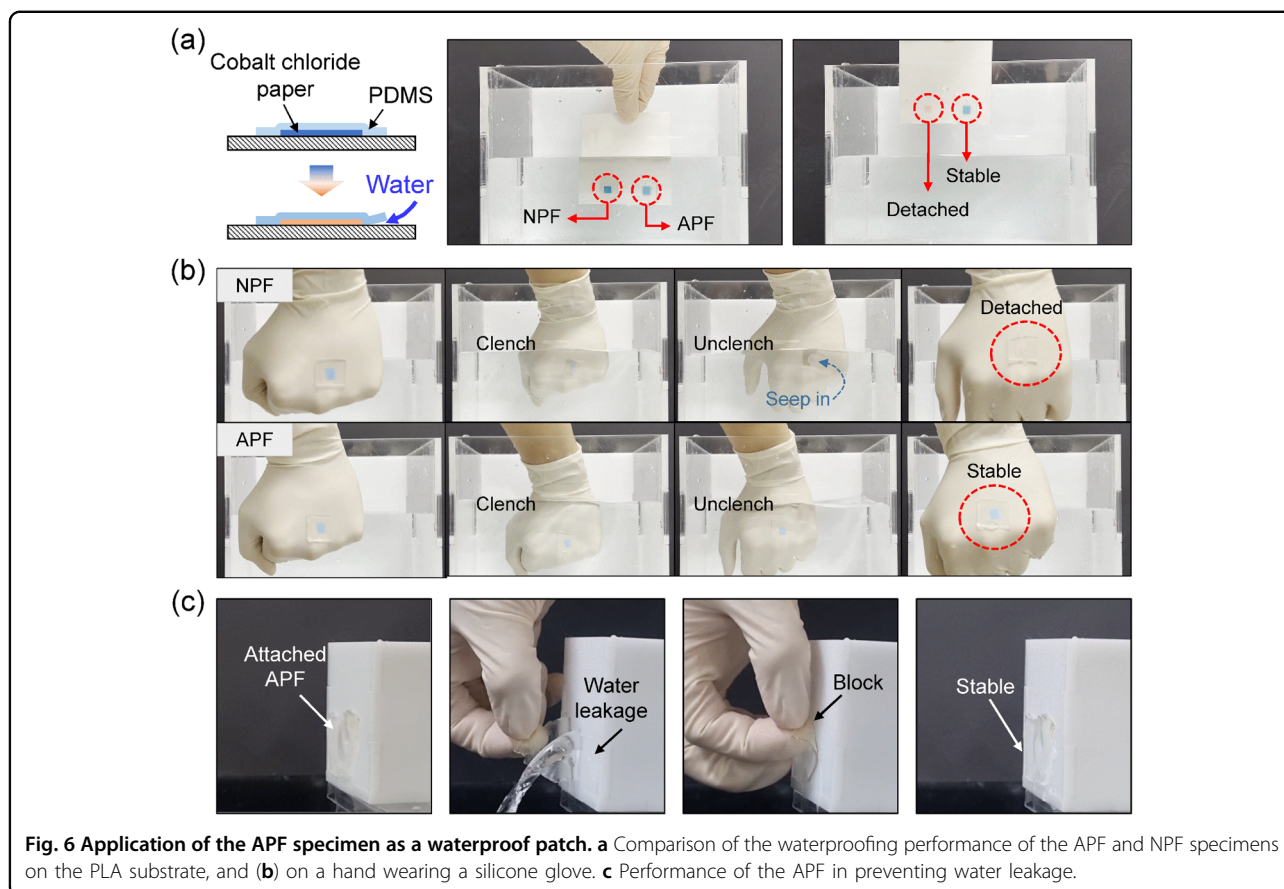


**Fig. 5 Underwater adhesion of the APF specimen.** **a** Water contact angles of different substrates including wafer, Al, and PLA. **b** Underwater adhesion strengths of the APF and NPF on different substrates. **c** Comparison of the adhesion strengths of the APF on different substrates under dry and underwater conditions. **d** Cyclic adhesion tests of the APF specimen under underwater conditions.

Al, and PLA substrates were selected as representative substrates for adhesion tests under wet conditions, and their CAs were 48.3°, 99.3°, and 103.8°, respectively. Thereafter, normal wet adhesion tests were conducted using an experimental setup similar to that used under dry conditions. An underwater environment was created by filling a transparent acrylic box with water and installing the desired substrates (Fig. S1c). Compared with the NPF, the APF demonstrated significantly stronger underwater adhesion on various substrates, as shown in Fig. 5b. APF exhibited underwater adhesion strengths of 12.0 kPa, 14.7 kPa, and 15.6 kPa on Si wafers, Al, and PLA substrates, respectively. In contrast, the NPF yielded underwater adhesion strengths of only 2.2 kPa, 0.8 kPa, and 0.9 kPa on the same substrates. This occurred because more dangling and free chains on the lightly cross-linked side of the APF increased the van der Waals force and allowed the APF to make contact more easily and adhere to the substrates<sup>18</sup>. Additionally, the APF adhered well to various substrates, including PET, Si wafers, glass, Al, PLA, and TPU, under water, as shown in Fig. S8c. Figure 5c shows a comparison of the adhesive strengths of the APFs in normal adhesion tests conducted under dry and wet conditions. In the case of an Al substrate with a comparatively large CA, the surface energy was lower than that of a Si wafer<sup>41,42</sup>. Materials with lower

surface energies exhibited resistance to adhesion due to poor wetting and chemical inertness<sup>43</sup>. Therefore, under dry conditions, adhesion of the APF on the Si wafer substrate was stronger than that on the Al substrate. However, a different trend was observed in wet environments. For the Al substrate, the adhesion strength in water was slightly lower than that for dry conditions, but excellent adhesion was still obtained. As shown in Fig. S9b, PDMS exhibited a CA of 108°, indicating its hydrophobicity. As the APF approached the Al substrate underwater, both the APF and the Al substrate exhibited hydrophobic properties, effectively repelling water at the interface. Subsequently, the high adhesion strength seen for the APF and the Al substrate was attributed to the lightly cross-linked side of the APF with many dangling and free chains. The increased mobilities of the chains facilitated easy and conformal contact between the APF and the substrate, thereby strengthening the van der Waals forces<sup>18</sup>. Therefore, compared to the dry environment, there was a minimal decrease in adhesion strength. In contrast, the adhesion strengths on the Si wafer substrate differed by more than 2.43 times for the dry and wet conditions. In this case, APF exhibited hydrophobic characteristics, while the Si wafer substrate was hydrophilic. As a result, compared to the Al substrate, the APF was unable to repel water at the interface with the Si wafer



substrate, ultimately leading to a substantial decrease in underwater adhesion strength<sup>9,44</sup>. An analysis of the results based on the CAs indicated that the difference in the adhesion strengths measured under dry and underwater conditions increased as the CA of the substrate decreased. Consequently, in underwater environments, the strength of APF adhesion on the Si wafer substrate was significantly lower than that on the Al substrate. This led to the conclusion that the hydrophobicity of the substrate was a critical factor influencing the underwater adhesive strength. To demonstrate reusability under wet conditions, cyclic tests were conducted for a total of 20 cycles, as shown in Fig. 5d. The results indicated that even with repeated use of water, the adhesion strengths remained stable, and no degradation occurred. In creep tests performed under water, the APF lasted for  $414.7 \pm 10.5$  s with a 200 g weight attached, indicating that it is suitable for underwater reuse. In conclusion, the APF is a hybrid adhesive film that exhibited excellent adhesion in both dry and underwater environments. This opens up promising possibilities for practical application.

#### Adhesive films for waterproof patches

To validate the applicability of the proposed APF, waterproofing tests were conducted in water on both a flat substrate and an unevenly gloved hand, as shown in Fig. 6. As shown in Fig. 6a, two pieces of cobalt chloride paper were attached to the PLA substrate, and the NPF and APF were applied to the top. The waterproofing performance of each PDMS film was assessed by observing the color change of the cobalt chloride paper. When the substrate was placed in a water chamber and shaken several times, the cobalt chloride paper with the NPF turned red, whereas the cobalt chloride paper with the APF remained blue, indicating no moisture penetration. Figure 6b shows additional adhesion tests performed under more challenging conditions, in which the film was attached to a silicone glove and the hand was moved. The NPF and APF were tested sequentially through repeated clenching and unclenching of the hand inside the water chamber while monitoring the color of the cobalt chloride paper. Similar to the results shown in Fig. 6a, the drag force with water caused the edges of the NPF to separate from the glove, allowing water to seep in and turn the cobalt chloride paper red. However, when the APF was adhered to the silicon glove, it maintained adhesion even with repeated hand movements, preventing water from permeating the APF and allowing the cobalt chloride paper to remain blue.



Furthermore, as shown in Fig. 6c, the APF was also used to prevent water leakage from a hole in an acrylic box. When the APF was initially adhered to the hole, the water did not leak and remained stable. However, once the APF was peeled off, water started to leak from the hole. Reattaching the APF to the hole stopped the water leakage and restored the stable state. These results demonstrated excellent adhesion of the APF under water, highlighting its potential for use as a waterproof patch and water-leakage sealing tape.

## Conclusion

In summary, we developed a novel adhesive PDMS film by casting PDMS on a TPU substrate. The side of the PDMS in contact with the TPU during the curing process was lightly cross-linked and exhibited a substantial increase in adhesion strength. The adhesive properties were analyzed using Raman spectroscopy and ICP-MS. The results showed that Pt depletion by the TPU inhibited PDMS curing, forming a lightly cross-linked side with a higher concentration of dangling and free chains. The obtained APFs exhibited exceptional adhesion on various substrates under both dry and underwater conditions. The experimental results confirmed that the APF showed stronger adhesion, approximately 13.6 times greater than that of the NPF, on the PLA substrate under dry conditions. Additionally, the adhesion performance remained stable even after multiple adhesion cycles, thus demonstrating its reusability. In an underwater environment, the APF showed excellent adhesion and repeatability on all substrates. As a practical application, the APF demonstrated its effectiveness as a waterproof patch by efficiently separating the water layer from the surface of an object upon attachment. Because the APF showed excellent adhesion in both dry and underwater environments, it is expected that the film can be used in various fields, such as in wearable electronic devices and health care, by utilizing these advantages.

## Supplementary materials

Material properties of the samples: Young's moduli and adhesion forces. Concentration of Pt atoms in the TPU film. Experimental setup for tensile and adhesion tests under both dry and underwater conditions. Adhesion strength with respect to displacement. Raman spectral analysis. The fabrication method for double PDMS and optical images of the condensed gel. Surface profiles of 3D-printed substrates with different printing resolutions. Contact area of the APF with the substrate depending on pressure. Optical images of APF adhering to various substrates. Contact angle on various substrates and the PDMS surface.

## Author contributions

S.P.: Conceptualization, Methodology, Formal analysis, Investigation, Data curation, Validation, Visualization, Writing—Original Draft, Writing—Review & Editing; M.K.: Conceptualization, Methodology, Formal analysis, Investigation, Data curation, Validation, Visualization, Writing—Original Draft, Writing—Review & Editing; H.S.:

Conceptualization, Methodology, Resources, Supervision, Writing—Review & Editing, Funding acquisition.

## Funding

This work was supported by the Korea Institute of Energy Technology Evaluation and Planning (KETEP) and the Ministry of Trade, Industry, and Energy (MOTIE) of the Republic of Korea (No. 20221A1010001B and 2020200000010).

## Conflict of interest

The authors declare no competing interests.

## Publisher's note

Springer Nature remains neutral with regard to jurisdictional claims in published maps and institutional affiliations.

**Supplementary information** The online version contains supplementary material available at <https://doi.org/10.1038/s41427-024-00546-8>.

Received: 13 October 2023 Revised: 26 February 2024 Accepted: 29 February 2024

Published online: 17 May 2024

## References

1. Autumn, K. et al. Adhesive force of a single gecko foot-hair. *Nature* **405**, 681–685 (2000).
2. Lee, B. P., Messersmith, P. B., Israelachvili, J. N. & Waite, J. H. Mussel-inspired adhesives and coatings. *Annu. Rev. Mater. Res.* **41**, 99–132 (2011).
3. Baik, S. et al. A wet-tolerant adhesive patch inspired by protuberances in suction cups of octopi. *Nature* **546**, 396–400 (2017).
4. Kim, D. W. et al. Highly permeable skin patch with conductive hierarchical architectures inspired by amphibians and octopi for omnidirectionally enhanced wet adhesion. *Adv. Funct. Mater.* **29**, 1807614 (2019).
5. Tan, D. et al. Robust and smart underwater adhesion of hydrophobic hydrogel by phase change. *Chem. Eng. J.* **471**, 144625 (2023).
6. Kim, D. H. et al. Epidermal electronics. *Science* **333**, 838–843 (2011).
7. Li, Q. et al. A biocompatible, self-adhesive, and stretchable photonic crystal sensor for underwater motion detection. *J. Mater. Chem. C* **10**, 9025–9034 (2022).
8. Chen, G. et al. Superstrong Water-Resistant underwater adhesives enabled by in situ coacervation through dense hydrogen bonds. *Chem. Eng. J.* **460**, 141691 (2023).
9. Wan, X. et al. Asymmetric Janus adhesive tape prepared by interfacial hydrosilylation for wet/dry amphibious adhesion. *NPG Asia Mater.* **11**, 49 (2019).
10. Seok, M., Choi, Y. & Cho, Y. Reusable and porous skin patches with thermopneumatic adhesion control capability and high water vapor permeability. <https://doi.org/10.1021/acsami.3c10603> (2023).
11. Yan, Y. et al. A strong underwater adhesive that totally cured in water. *Chem. Eng. J.* **431**, 133460 (2022).
12. Xu, W. & Wei, Y. Strength and interface failure mechanism of adhesive joints. *Int. J. Adhes. Adhes.* **34**, 80–92 (2012).
13. Yi, M.-B. et al. Movable cross-linking in adhesives: superior stretching and adhesion properties via a supramolecular sliding effect. *ACS Appl. Polym. Mater.* **3**, 2678–2686 (2021).
14. Cho, S. et al. Large-area cross-aligned silver nanowire electrodes for flexible, transparent, and force-sensitive mechanochromic touch screens. *ACS Nano* **11**, 4346–4357 (2017).
15. Park, S., Bang, J. & So, H. 3D printing-assisted and magnetically-actuated superhydrophobic surfaces for droplet control. *Surf. Interfaces* **37**, 102678 (2023).
16. Cheng, J. et al. Wet-adhesive elastomer for liquid metal-based conformal epidermal electronics. *Adv. Funct. Mater.* **32**, 2200444 (2022).
17. Yan, C. et al. Highly stretchable piezoresistive graphene-nanocellulose nanopaper for strain sensors. *Adv. Mater.* **26**, 2022–2027 (2014).
18. Gu, Z. et al. Skin adhesives with controlled adhesion by polymer chain mobility. *ACS Appl. Mater. Interfaces* **11**, 1496–1502 (2019).

19. Cui, C. & Liu, W. Recent advances in wet adhesives: adhesion mechanism, design principle and applications. *Prog. Polym. Sci.* **116**, 101388 (2021).
20. Hu, P., Madsen, J. & Skov, A. L. One reaction to make highly stretchable or extremely soft silicone elastomers from easily available materials. *Nat. Commun.* **13**, 370 (2022).
21. Jeong, S. H., Zhang, S., Hjort, K., Hilborn, J. & Wu, Z. PDMS-based elastomer tuned soft, stretchable, and sticky for epidermal electronics. *Adv. Mater.* **28**, 5830–5836 (2016).
22. Johnston, I. D., McCluskey, D. K., Tan, C. K. L. & Tracey, M. C. Mechanical characterization of bulk Sylgard 184 for microfluidics and microengineering. *J. Micromech. Microeng.* **24**, 035017 (2014).
23. Venzac, B. et al. PDMS curing inhibition on 3d-printed molds: why? also, how to avoid it? *Anal. Chem.* **93**, 7180–7187 (2021).
24. Kim, J.-H., Kim, S.-R., Kil, H.-J., Kim, Y.-C. & Park, J.-W. Highly conformable, transparent electrodes for epidermal electronics. *Nano Lett.* **18**, 4531–4540 (2018).
25. Carlborg, C. F., Haraldsson, T., Cornaglia, M., Stemme, G. & van der Wijngaart, W. A high-yield process for 3-d large-scale integrated microfluidic networks in PDMS. *J. Microelectromech. Syst.* **19**, 1050–1057 (2010).
26. Fan, H. & Gong, J. P. Bioinspired underwater adhesives. *Adv. Mater.* **33**, 2102983 (2021).
27. Sabourault, N., Mignani, G., Wagner, A. & Mioskowski, C. Platinum oxide (PtO<sub>2</sub>): a potent hydrosilylation catalyst. *Org. Lett.* **4**, 2117–2119 (2002).
28. Hamze, A., Provot, O., Alami, M. & Brion, J.-D. Platinum oxide catalyzed hydrosilylation of unsymmetrical internal aryl alkynes under ortho-substituent regiocontrol. *Org. Lett.* **7**, 5625–5628 (2005).
29. Venkatachalam, S. & Hourlier, D. Heat treatment of commercial Polydimethylsiloxane PDMS precursors: Part I. Towards conversion of patternable soft gels into hard ceramics. *Ceram. Int.* **45**, 6255–6262 (2019).
30. Hanada, S., Tsutsumi, E., Motoyama, Y. & Nagashima, H. Practical access to amines by platinum-catalyzed reduction of carboxamides with hydrosilanes: synergy of dual Si–H groups leads to high efficiency and selectivity. *J. Am. Chem. Soc.* **131**, 15032–15040 (2009).
31. Gu, Z. et al. Crosslinking-dependent relaxation dynamics in ethylene–propylene–diene (EPDM) terpolymer above the glass transition temperature. *J. Macromol. Sci. B* **54**, 618–627 (2015).
32. Esteves, A. C. C. et al. Influence of cross-linker concentration on the cross-linking of PDMS and the network structures formed. *Polymer* **50**, 3955–3966 (2009).
33. Bruckmoser, K. & Resch, K. Investigation of ageing mechanisms in thermoplastic polyurethanes by means of IR and Raman spectroscopy. *Macromol. Symp.* **339**, 70–83 (2014).
34. Cai, D., Neyer, A., Kuckuk, R. & Heise, H. M. Raman, mid-infrared, near-infrared and ultraviolet–visible spectroscopy of PDMS silicone rubber for characterization of polymer optical waveguide materials. *J. Mol. Struct.* **976**, 274–281 (2010).
35. Kalaivani, S. S., Muthukrishnaraj, A., Sivanesan, S. & Ravikumar, L. Novel hyperbranched polyurethane resins for the removal of heavy metal ions from aqueous solution. *Process Saf. Environ. Prot.* **104**, 11–23 (2016).
36. Weakley, A. T., Warwick, P. C. T., Bitterwolf, T. E. & Aston, D. E. Multivariate analysis of micro-Raman spectra of thermoplastic polyurethane blends using principal component analysis and principal component regression. *Appl. Spectrosc.* **66**, 1269–1278 (2012).
37. Eklund, A., Ikkala, O. & Zhang, H. Highly efficient switchable underwater adhesion in channeled hydrogel networks. *Adv. Funct. Mater.* **2214091**, 1–12 (2023).
38. Michaelis, M. & Leopold, C. S. A measurement system analysis with design of experiments: Investigation of the adhesion performance of a pressure sensitive adhesive with the probe tack test. *Int. J. Pharm.* **496**, 448–456 (2015).
39. Zhao, K., Hu, Z., Wang, B., Li, Q. & Xu, Y. Effect of roughness and adhesive on the strength of concrete-to-concrete interfaces cast from 3D-printed prefabricated plastic formworks. *Constr. Build. Mater.* **368**, 130423 (2023).
40. Tahir, A. et al. Improving WC-Co coating adhesive strength on rough substrate: finite element modeling and experiment. *J. Mater. Sci. Technol.* **37**, 1–8 (2020).
41. Crick, C. R. & Parkin, I. P. Preparation and characterisation of super-hydrophobic surfaces. *Chem.—Eur. J.* **16**, 3568–3588 (2010).
42. Jothi Prakash, C. G. & Prasanth, R. Approaches to design a surface with tunable wettability: a review on surface properties. *J. Mater. Sci.* **56**, 108–135 (2021).
43. Huang, S. et al. Adhering low surface energy materials without surface pretreatment via ion-dipole interactions. *ACS Appl. Mater. Interfaces* **13**, 41112–41119 (2021).
44. Zhou, J., Anim-Danso, E., Zhang, Y., Zhou, Y. & Dhinojwala, A. Interfacial water at polyurethane–sapphire interface. *Langmuir* **31**, 12401–12407 (2015).